

## THE $r$ -PROCESS IN PROTO-NEUTRON-STAR WIND REVISITED

SHINYA WANAJO<sup>1</sup>

*Draft version October 11, 2018*

### ABSTRACT

We examine the  $r$ -process in the neutrino-driven proto-neutron-star (PNS) wind of core-collapse supernovae in light of the recent findings of massive neutron stars in binaries as well as of an indication of neutron-richness in the PNS ejecta because of the nucleon potential corrections on neutrino opacities. To this end, a spherically symmetric, general relativistic, steady-state wind model is applied for a wide range of PNS masses between  $1.2M_{\odot}$  and  $2.4M_{\odot}$  with the latter reaching the causality limit. Nucleosynthesis calculations with these PNS models are performed by assuming a time evolution of electron fraction with its minimal value of  $Y_e = 0.4$ , which mimics recent hydrodynamical results. The fundamental nucleosynthetic aspect of the PNS wind is found to be the production of Sr, Y and Zr in quasi-equilibrium and of the elements with  $A \approx 90$ –110 by a weak  $r$ -process, which can be an explanation for the abundance signatures in  $r$ -process-poor Galactic halo stars. PNSs more massive than  $2.0M_{\odot}$  can eject heavy  $r$ -process elements, however, with substantially smaller amount than what is needed to account for the solar content. PNS winds can be thus the major origin of light trans-iron elements but no more than 10% of those heavier than  $A \sim 110$ , although they may be the sources of the low-level abundances of Sr and Ba found in numerous metal-poor stars if the maximum mass of PNSs exceeds  $2.0M_{\odot}$ .

*Subject headings:* nuclear reactions, nucleosynthesis, abundances — stars: abundances — supernovae: general

### 1. INTRODUCTION

Proto-neutron-star (PNS) wind of core-collapse supernovae (CCSNe), the outflows driven by neutrino heating, has long been suggested to be the major site of the  $r$ -process (rapid neutron-capture process) since early 1990's (Meyer et al. 1992; Woosley et al. 1994). One of the problems in these early works was the very high entropy in the wind,  $S \sim 400 k_B \text{ nucleon}^{-1}$  ( $k_B$  is the Boltzmann constant), which was not confirmed by subsequent works ( $S \sim 100 k_B \text{ nucleon}^{-1}$ , Takahashi et al. 1994; Qian & Woosley 1996). General relativistic effects were found to increase entropy (Cardall & Fuller 1997) but needed a PNS more massive than  $M \approx 2.0M_{\odot}$  for robust  $r$ -processing (Otsuki et al. 2000; Wanajo et al. 2001; Thompson et al. 2001). Another problem was an unacceptable overproduction of some species such as Sr, Y, and Zr (Woosley et al. 1994; Wanajo et al. 2001). More seriously, hydrodynamical simulations of CCSNe with elaborate neutrino transport indicated proton-richness in the wind ejecta (Fischer et al. 2010; Hudepohl et al. 2010). These works seemed to exclude the PNS wind scenario as the  $r$ -process site.

Recent works on the effect of nucleon potential corrections for neutrino opacities seem, in part, to revive the PNS wind scenario (Reddy et al. 1998; Roberts 2012; Martínez-Pinedo et al. 2012; Roberts et al. 2012; Horowitz et al. 2012). These works predict that the electron fraction ( $Y_e$ ; number of protons per nucleon) drops off from an initially proton-rich value to the minimal value of  $\sim 0.42$ – $0.45$  and increases again towards  $\sim 0.5$  in the late wind phase, the behavior not expected in previous works. Recent discoveries of massive NSs in binary

systems with a precision measurement of  $M = 1.97 \pm 0.04M_{\odot}$  for PSR J1614-2230 (Demorest et al. 2010) and an inferred mass of  $M \sim 2.4M_{\odot}$  for PSR B1957+20 (van Kerkwijk et al. 2011) are also encouraging for the PNS wind scenario.

In this Letter we aim to revisit the issue of the  $r$ -process in PNS winds in light of these recent findings. This is to extend and improve the previous nucleosynthesis studies, which were based on limited hydrodynamical outcomes (e.g., Woosley et al. 1994; Arcones & Montes 2011) or semi-analytic solutions with a few selected parameter sets (e.g.,  $M = 1.4M_{\odot}$  and  $2.0M_{\odot}$ ; Wanajo et al. 2001) with  $Y_e$  evolutions that were incompatible with the recent works. To this end, a semi-analytical wind model (Wanajo et al. 2001) is applied for a wide range of  $M$  between  $1.2M_{\odot}$  and  $2.4M_{\odot}$  (Section 2). Nucleosynthesis calculations are performed with the wind solutions by assuming a time evolution of  $Y_e$  (Section 3) that mimics the result of Roberts et al. (2012). The nucleosynthesis yields are mass-integrated to compare with the solar  $r$ -process abundances as well as those in Galactic halo stars. We then discuss whether PNS winds can be the sources of  $r$ -process elements in the Galaxy.

### 2. WIND MODEL

Although the underlying physics what causes the explosions of CCSNe has been under debate (e.g., Janka et al. 2012), it is known that the neutrino-driven outflows after evacuation of the early convective ejecta are well described by the steady-state (semi-) analytical solutions of PNS wind models (Duncan et al. 1986; Qian & Woosley 1996; Cardall & Fuller 1997; Otsuki et al. 2000; Wanajo et al. 2001; Thompson et al. 2001). In this study, we use the spherically symmetric, general relativistic, semi-analytic wind model in Wanajo et al. (2001, for more detail, see their Section 2).

<sup>1</sup> National Astronomical Observatory of Japan, 2-21-1 Osawa, Mitaka, Tokyo 181-8588, Japan; shinya.wanajo@nao.ac.jp

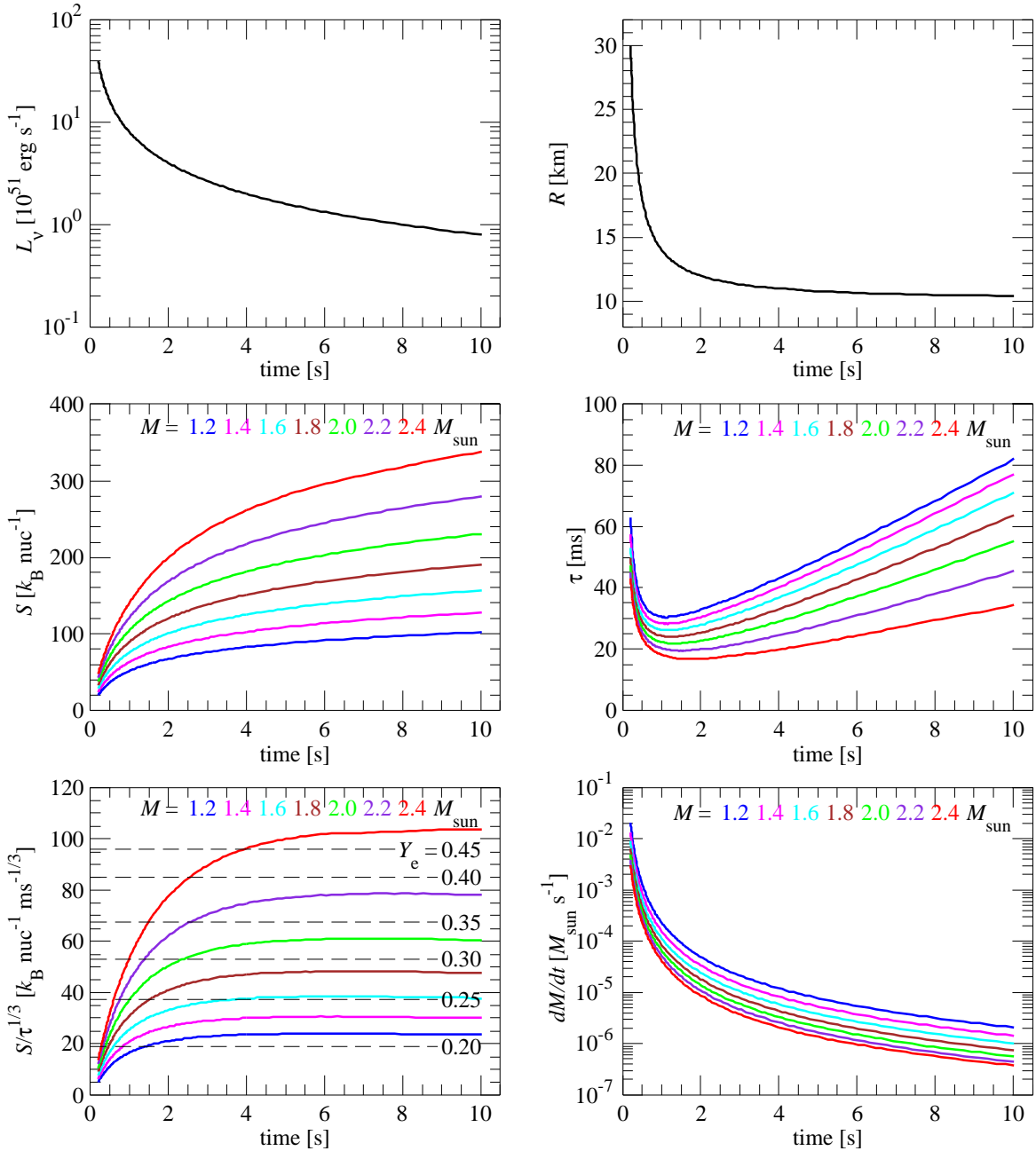


FIG. 1.— Time evolutions of  $L_\nu$  (top left) and  $R$  (top right) adopted in this study. Resulting  $S$  (middle left),  $\tau$  (middle right),  $S/\tau^{1/3}$  (bottom left), and  $\dot{M}$  (bottom right) are shown as functions of  $t$ . In the bottom-left panel, the  $Y_e$ 's, above which the production of  $A \sim 200$  nuclei are predicted, are indicated by dashed lines.

The average neutrino energies are taken to be 12, 14, and 14 MeV for electron neutrino, electron antineutrino, and heavy lepton neutrinos, respectively (according to, e.g., Fischer et al. 2010; Hüdepohl et al. 2010). The equation of state for ions (ideal gas) and arbitrarily degenerate, arbitrarily relativistic electrons and positrons is taken from Timmes & Swesty (2000).

Each wind (i.e., transonic) solution can be obtained for a given set of  $(M, R, L_\nu)$ ; we assume the PNS radius  $R$  to be the same as the neutrinosphere and the neutrino luminosities of all the flavors to have the same value  $L_\nu$ . We consider the models of  $M/M_\odot = 1.2, 1.4, 1.6, 1.8, 2.0, 2.2,$  and  $2.4$ , which cover the range of measured and estimated masses of NSs (Demorest et al.

2010; van Kerkwijk et al. 2011; Lattimer 2011). For  $L_\nu$  and  $R$ , phenomenological time evolutions during the first 10 s after core bounce ( $t_0 = 0.20 \text{ s} \leq t \leq t_1 = 10 \text{ s}$ ) are adopted as follows. To roughly mimic recent results of long-term simulations over the PNS cooling phase (e.g., Fischer et al. 2010; Hüdepohl et al. 2010), we assume  $L_\nu(t) = L_{\nu,0}(t/t_0)^{-1}$  with  $L_{\nu,0} (\text{erg s}^{-1}) = 10^{52.4} = 3.98 \times 10^{52}$  (Fig. 1; top left). We also assume  $R(L_\nu) = (R_0 - R_1)(L_\nu/L_{\nu,0}) + R_1$  with  $R_0 = 30 \text{ km}$  and  $R_1 = 10 \text{ km}$  so that each wind solution can be obtained from a given set of  $(M, L_\nu)$ . This is equivalent to set  $R(t) = (R_0 - R_1)(t/t_0)^{-1} + R_1$  (Fig. 1; top right). Note that  $R(t_1) = 10.4 \text{ km}$  matches the lower

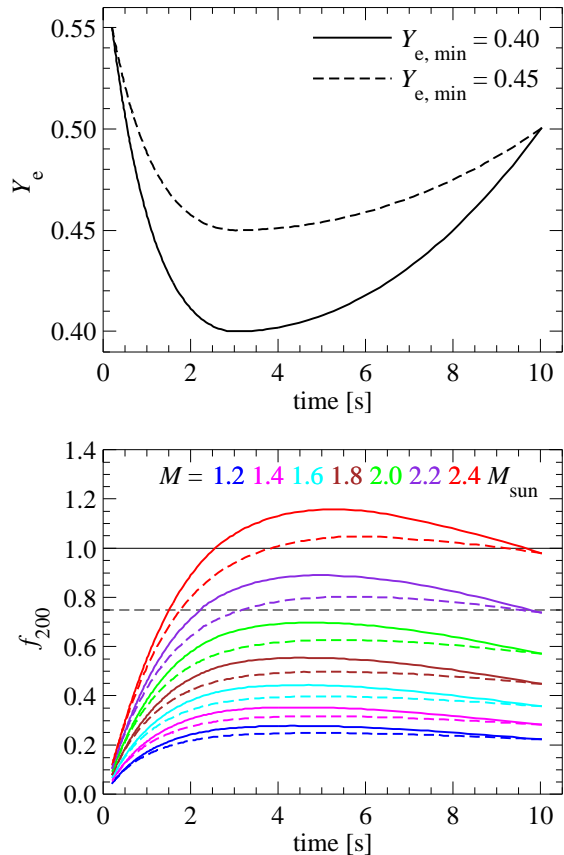


FIG. 2.— Top: time evolution of  $Y_e$  adopted for nucleosynthesis calculations ( $Y_{e,\min} = 0.40$ ; solid curve). The case with  $Y_{e,\min} = 0.45$  is also shown by the dashed curve. Bottom: values of  $f_{200}$  (Eq. [1]) as functions of  $t$ . The cases for  $Y_{e,\min} = 0.40$  and  $0.45$  are shown by solid and dashed curves, respectively. The solid and dashed horizontal lines indicate  $f_{200} = 1$  and  $f_{130} = 1$ , respectively, above which the production of  $A \sim 200$  and  $A \sim 130$  nuclei are expected.

bound of the constraint for cold NSs (with  $M = 1.4M_\odot$ ),  $10.4 \text{ km} \leq R \leq 12.9 \text{ km}$ , inferred by Steiner et al. (2013). With this assumption, the  $2.4M_\odot$  model reaches the smallest radius ( $\approx 10.3 \text{ km}$ ) allowed by the causality limit (the speed of sound must not exceed the speed of light),  $R \gtrsim 4.3(M/M_\odot) \text{ km}$  (Lattimer 2011). The PNS with  $M = 2.4M_\odot$  should be thus taken as the absolute extreme model.<sup>2</sup>

Wind solutions for each  $M$  model are computed for  $\log L_\nu(\text{erg s}^{-1}) = 52.60, 52.59, \dots, 50.90$  ( $t_0 \leq t \leq t_1$ ;  $171 L_\nu$ 's). The middle and bottom panels (Fig. 1) illustrate the resulting basic properties. We confirm the previous results (Otsuki et al. 2000; Wanajo et al. 2001; Thompson et al. 2001) that the asymptotic entropy ( $S$ ; middle left) increases with time, being systematically greater for more massive PNSs. We further find a strong sensitivity of  $S$  to  $M$  for  $> 2.0M_\odot$ , which reaches  $338 k_B \text{ nucleon}^{-1}$  for  $M = 2.4M_\odot$ . This is a consequence of the general relativistic effects that are particularly important when  $M/R$  is close to the causality limit (Cardall & Fuller 1997). We also find systemati-

cally smaller expansion timescales ( $\tau$ ; defined as the  $e$ -folding time of temperature below  $0.5 \text{ MeV}$ , Otsuki et al. 2000) for more massive PNSs, which take minimal values at  $t \sim 1\text{--}2 \text{ s}$  and increase with time (Fig. 1; middle right).

As analytically shown by Hoffman et al. (1997), the ratio  $S/\tau^{1/3}$  (with a fixed  $Y_e$ ) serves as the measure of the strength of  $r$ -processing. We find in the bottom-left panel (Fig. 1) that  $S/\tau^{1/3}$  increases with time and saturates at  $t \sim 5 \text{ s}$  as a result of the increasing  $\tau$  that counterbalances the increasing  $S$ . That is, the strength of  $r$ -processing becomes mostly independent of time for  $t \gtrsim 5 \text{ s}$  if  $Y_e$  is kept constant. The dashed lines indicate the values of  $Y_e$  above which the production of  $A \sim 200$  nuclei are expected, according to the analytical formula in Hoffman et al. (1997, their Eq. (19)). We find that an unacceptably low  $Y_e (< 0.25)$  is required for  $M = 1.4M_\odot$ . If a currently predicted minimal value of  $Y_e \sim 0.42\text{--}0.45$  were taken, one would need a PNS with the mass close to the extreme case of  $M = 2.4M_\odot$  for the production of heavy  $r$ -process nuclei.<sup>3</sup> The bottom-right panel shows the mass ejection rates ( $\dot{M}$ ) that are systematically smaller for more massive PNS models and quickly decrease with time. This indicates that the wind ejecta are dominated by the early components with small  $S/\tau^{1/3}$ . The very late ejecta for  $t > 10 \text{ s}$  (if any; not considered in this study) would be unimportant.

The time evolution of  $Y_e$ , which is needed for nucleosynthesis calculations, is assumed as  $Y_e(t) = c_1 \cosh[c_2(t - t_{\min})] + c_3$  (Fig. 2; top), where  $c_2 = 1.0$  for  $t < t_{\min} = 3.0 \text{ s}$  and  $c_2 = 0.10$  for  $t > t_{\min}$ . The coefficients  $c_1$  and  $c_3$  are determined to satisfy  $Y_e(t_{\min}) = Y_{e,\min}$  and, for  $t < t_{\min}$  and  $t > t_{\min}$ , respectively,  $Y_e(t_0) = 0.55$  and  $Y_e(t_1) = 0.50$ . This roughly mimics the hydrodynamical result by Roberts et al. (2012, see their Fig. 5). We adopt  $Y_{e,\min} = 0.40$  (solid curve in the top panel of Fig. 2), the value slightly smaller than  $\sim 0.42\text{--}0.45$  in Roberts et al. (2012). While  $Y_e$  drops in response to the PNS contraction, the increasing neutrinospheric density suppresses the charged current neutrino interactions by Pauli blocking and  $Y_e$  cannot decrease at late times (Fischer et al. 2012). Note that the  $\alpha$ -effect (McLaughlin et al. 1996; Meyer et al. 1998), which were not considered in Roberts et al. (2012), would slightly shift  $Y_e$  towards  $\sim 0.5$ . The value of  $Y_{e,\min}$  here may thus be taken as the absolute lower limit for PNS winds.

The lower panel (Fig. 2) shows the condition for making the third peak nuclei ( $A \sim 200$ ) according to Hoffman et al. (1997),

$$f_{200} = \frac{(S/230 k_B \text{ nucleon}^{-1})}{(Y_e/0.40)(\tau/20 \text{ ms})^{1/3}} \gtrsim 1, 0.38 \lesssim Y_e \lesssim 0.46(1)$$

This reflects the value of  $Y_e$  in addition to the combination  $S/\tau^{1/3}$  (Fig. 1; bottom left). We find that only the extreme model of  $M = 2.4M_\odot$  satisfies this condition (the region above the horizontal solid line). Also indicated by the horizontal dashed line is the con-

<sup>2</sup> Wanajo et al. (2001) showed that, with inclusion of general relativistic effects, nucleosynthetic outcomes were roughly scaled with  $M/R$ . Nucleosynthetic results of  $M/M_\odot = 1.2\text{--}2.4$  with  $R_1 = 10 \text{ km}$  here would be thus similar to those of, e.g.,  $M/M_\odot = 1.4\text{--}2.9$  with  $R_1 = 12 \text{ km}$ .

<sup>3</sup> Otsuki et al. (2000) and Wanajo et al. (2001) showed that the wind of  $(M, L_\nu) = (2.0M_\odot, 10^{52} \text{ erg s}^{-1})$  with  $Y_e = 0.40$  led to a robust  $r$ -process. Their PNS radius was, however, fixed to  $10 \text{ km}$ , which was appreciably smaller than our more reasonable, time-dependent value of  $R(L_\nu = 10^{52} \text{ erg s}^{-1}) = 15 \text{ km}$ .

TABLE 1  
EJECTA MASSES (IN UNITS OF  $10^{-5}M_{\odot}$ )

$M/M_{\odot}$	1.2	1.4	1.6	1.8	2.0	2.2	2.4
total	219	143	100	74.1	56.7	44.6	36.0
${}^4\text{He}$	122	92.7	71.9	56.9	45.8	37.4	31.0
$A > 100$	2.19	2.75	2.76	2.27	1.78	1.37	0.893
Sr	3.61	1.92	1.09	0.627	0.346	0.177	0.0764
Ba	0.00	0.00	0.00	0.00	0.0420	0.0373	0.0199
Eu	0.00	0.00	0.00	0.00	0.00452	0.00585	0.00305

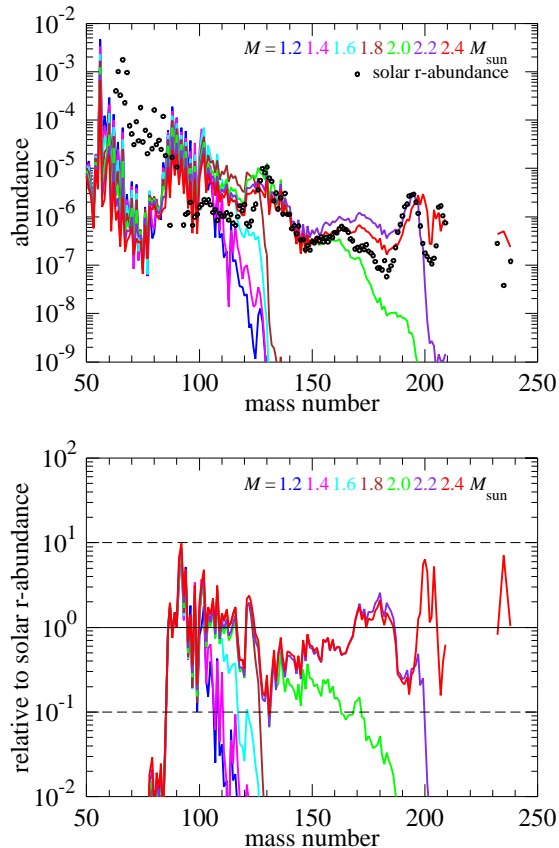


FIG. 3.— Top: mass-integrated nuclear abundances, which are compared with the solar  $r$ -process abundances (circles) that shifted to match the third peak height ( $A \sim 200$ ) for the  $2.4M_{\odot}$  model. Bottom: ratios of mass-integrated abundances relative to the solar  $r$ -process abundances (scaled at  $A = 90$ ).

dition for making the second peak ( $A \sim 130$ ) nuclei,  $f_{130} \approx 1.34 f_{200} \gtrsim 1$ . It indicates that only the models with  $M \gtrsim 2.0M_{\odot}$  can reach the second peak of the  $r$ -process abundances. The  $f_{200}$  curves with  $Y_{e,\min}$  replaced by 0.45 are also shown in Figure 2, implying slightly weaker  $r$ -processing.

### 3. NUCLEOSYNTHESIS

The nucleosynthetic yields for all the  $(M, L_{\nu})$  sets are computed with the reaction network code described in Wanajo et al. (2001, 2011b). Reaction rates are employed from the latest library of REACLIB V2.0 (Cyburt et al. 2010) for the experimental evaluations when available and the rest from the theoretical estimates in BRUSLIB (Xu et al. 2013) based on the HFB-21 mass predictions (Goriely et al. 2010). The  $\beta$ -decay rates are taken from the gross theory predictions

(GT2 Tachibana et al. 1990) obtained with the HFB-21 masses. Neutrino interactions, which would slightly shift  $Y_e$  by the  $\alpha$ -effect, are not included. Using thermodynamic trajectories of PNS winds, the calculations are started when the temperature decreases to 10 GK, assuming initially free protons and neutrons with mass fractions  $Y_e$  and  $1 - Y_e$ , respectively.<sup>4</sup>

The nucleosynthetic abundances are mass-integrated (Fig. 3; top) by adopting  $\dot{M}$  for each PNS model. For comparison purposes, the solar  $r$ -process compositions (circles) are also plotted to match the third peak height ( $A \sim 195$ ) for the  $M = 2.4M_{\odot}$  model. As anticipated from the lower panel of Figure 2, only the extreme model of  $M = 2.4M_{\odot}$  satisfactorily accounts for the production of heavy  $r$ -process nuclei up to Th ( $A = 232$ ) and U ( $A = 235$  and 238). The  $2.2M_{\odot}$  model reaches the third peak abundances but those beyond. The  $2.0M_{\odot}$  model reaches the second ( $A \sim 130$ ) but the third peak abundances. We find no strong  $r$ -processing for the models with  $M < 2.0M_{\odot}$ .

We find, however, quite robust abundance patterns below  $A \sim 110$ , which appears a fundamental aspect of nucleosynthesis in PNS winds. The double peaks at  $A \approx 56$  and 90 with a trough between them are formed in quasi-nuclear equilibrium (QSE;  $\gtrsim 4$  GK). Note also that the overproduction of  $N = 50$  species  ${}^{88}\text{Sr}$ ,  ${}^{89}\text{Y}$ ,  ${}^{90}\text{Zr}$  (Woosley et al. 1994; Wanajo et al. 2001) are not prominent in our result. This is due to the short duration of moderate  $S$  ( $< 100 k_B$  nucleon $^{-1}$ ; Fig. 1) with  $Y_e \sim 0.45$  (Fig. 3), in which the  $N = 50$  species copiously form in QSE. The lower panel of Figure 3 shows the ratios of nucleosynthetic abundances relative to their solar  $r$ -process values (normalized at  $A = 90$ ). For  $2.2M_{\odot}$  and  $2.4M_{\odot}$  models, the ratios are more or less flat between  $A = 90$  and 200, although deviations from unity are seen everywhere.

Table 1 provides the masses (in units of  $10^{-5}M_{\odot}$ ) of the total ejecta,  ${}^4\text{He}$ , those with  $A > 100$ , Sr, Ba, and Eu, for all the PNS models. The total ejecta masses span a factor of 6 with smaller values for more massive PNSs. The larger fractions of  ${}^4\text{He}$  in more massive models, however, lead to the ejecta masses for  $A > 100$  (total masses of  $r$ -process nuclei) ranging only a factor of 2.5. The masses of Sr range a factor of 50 with the greater amount for less massive models. Ba and Eu are produced only in the massive models with  $M \geq 2.0M_{\odot}$ .

Studies of Galactic chemical evolution estimate the average mass of Eu per CCSN event (if they were the origin) to be  $\sim 10^{-7}M_{\odot}$  (Ishimaru & Wanajo 1999), that is,  $\sim$  a few  $10^{-5}M_{\odot}$  for the nuclei with  $A > 100$ . Taken at the face value, the Eu masses for  $M \geq 2.0M_{\odot}$  reach 30%–60% of this requirement. The fraction of events with such massive PNSs would be limited to no more than  $\sim 20\%$  of all CCSN events (e.g.,  $\gtrsim 25M_{\odot}$ ). The masses of Eu from these massive PNSs are, therefore, about 10 times smaller than the requirement from Galactic chemical evo-

<sup>4</sup> We examined only the  $Y_{e,\min} = 0.40$  case with  $t_{\min} = 3.0$  s. Tests showed that a small shift of  $t_{\min}$  did not qualitatively change our result. The cases with  $Y_{e,\min} = 0.45$  corresponded to roughly re-scaling  $M$ 's with  $\sim 0.1$ – $0.2M_{\odot}$  smaller values. Note also that the presence of the preceding SN ejecta that give rise to the termination-shocks (Arcones et al. 2007) do not change the gross abundance features (Wanajo 2007; Kuroda et al. 2008).

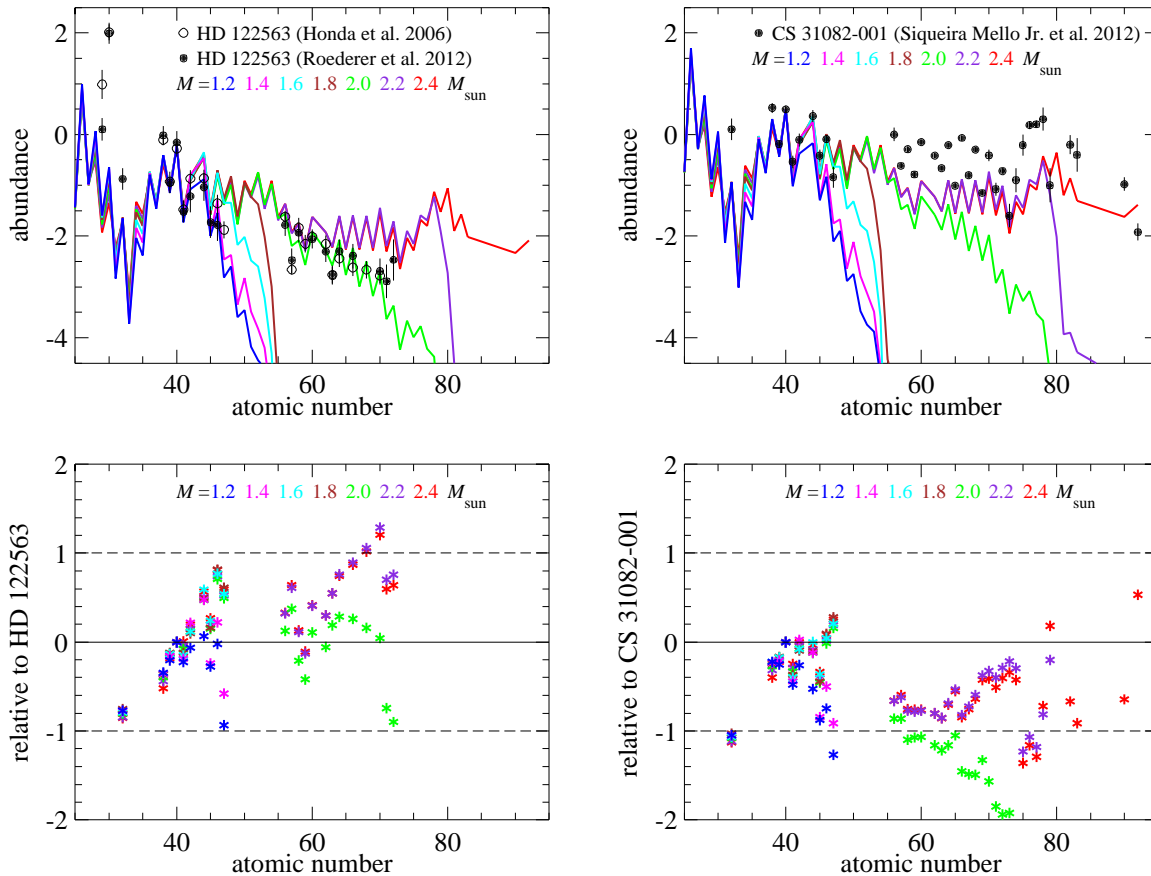


FIG. 4.— Mass-integrated elemental abundances compared to the stellar abundances (top panels) and their ratios (bottom panels). Two Galactic halo stars, HD 122563 (left, Honda et al. 2006; Roederer et al. 2012) and CS 31082-001 (right Siqueira Mello Jr. et al. 2013) are taken as representative of *r*-process-poor/rich stars, respectively. The nucleosynthetic abundances are normalized at  $Z = 40$ .

lution (the same holds for Ba). Note that, for massive PNS cases, the ejecta masses would be further reduced by fallback or black-hole formation (Qian et al. 1998; Boyd et al. 2012). For Sr, the required mass per CCSN event is estimated to be  $\sim 2 \times 10^{-6} M_{\odot}$  from the solar *r*-process ratio of Sr/Eu = 16.4 (Snedden et al. 2008). The low mass PNS models, which may represent the majority of CCSNe, thus overproduce Sr by about a factor of 10. The amount of QSE products such as Sr, Y, and Zr is, however, highly dependent on the multi-dimensional  $Y_e$  distribution in early times ( $t < 1$  s, Wanajo et al. 2011a).

Figure 4 compares the mass-integrated abundances with those of Galactic halo stars. Two well known objects are taken as representative of *r*-process-poor (HD 122563, left panels; Honda et al. 2006; Roederer et al. 2012) and *r*-process-rich (CS 31082-001, right panels; Siqueira Mello Jr. et al. 2013) stars with the metallicities  $[\text{Fe}/\text{H}] = -2.7$  and  $-2.9$ , respectively. These stars have  $[\text{Eu}/\text{Fe}] = -0.52$  and  $+1.69$ , respectively, well below and above the average value of  $\approx +0.5$  at  $[\text{Fe}/\text{H}] \approx -3$ . The top and bottom panels show, respectively, the mass-integrated abundances and their ratios relative to the stellar abundances, which are normalized to the stellar abundances at  $Z = 40$ .

In the left panels, we find that the  $1.2 M_{\odot}$  and  $1.4 M_{\odot}$  models result in reasonable agreement with the stellar abundances between  $Z = 38$  (Sr) and  $Z = 48$  (Cd). The  $2.0 M_{\odot}$  model nicely reproduces the abundance pattern of HD 122563 up to  $Z = 68$  (Er) but somewhat overpro-

duces the elements of  $Z = 46-48$  (Pd, Ag, Cd). It could be thus possible to interpret that the abundance signatures of *r*-process-poor stars were due to a weak *r*-process that reaches  $Z \sim 50$  ( $M < 2.0 M_{\odot}$ ) or  $70$  ( $M = 2.0 M_{\odot}$ ) with or without additional sources for  $Z > 50$ , respectively. In the right panels, we find that the stellar abundances between  $Z = 38$  (Sr) and  $Z = 47$  (Ag) are well reproduced by massive models with  $M \geq 1.6 M_{\odot}$ . The models with  $M = 2.2 M_{\odot}$  and  $2.4 M_{\odot}$  produce the heavier elements with a similar pattern to that of CS 31082-001 but with a smaller ratio. Because of the insufficient production of Eu (Table 1), our PNS models would not account for the high  $[\text{Eu}/\text{Fe}]$  value in this star. The winds from such massive PNSs ( $M \gtrsim 2.0 M_{\odot}$ ) could be, however, still the source of the low-level abundances (factor of several 10 smaller than the average values) of Sr and Ba in numerous metal-poor stars (Roederer 2013; Aoki et al. 2013).

#### 4. CONCLUSION

We revisited the issue of the *r*-process in neutrino-driven PNS winds in light of recent findings of the massive NSs as well as of the neutron-richness in the PNS ejecta. Nucleosynthesis calculations were performed with the semi-analytical wind models over a wide range of the PNS masses ( $1.2 \leq M/M_{\odot} \leq 2.4$ ), assuming a phenomenological time evolutions of  $Y_e$ .

Based on our result, including the extreme model ( $M = 2.4 M_{\odot}$ ) that encounters the causality limit, it

would be safe to conclude that neutrino-driven PNS winds were excluded as the major origin of heavy  $r$ -process elements. Note that some previous works have suggested several mechanisms that help to increase  $S$  and reduce  $\tau$ , e.g., strong magnetic field (Thompson 2003; Suzuki & Nagataki 2005) and highly anisotropic neutrino emission (Wanajo 2006). Our conclusion would not be changed if such mechanisms (associated to probably rare events) were considered, as far as the dominant driving source of the wind is neutrino heating (which sets  $\dot{M}$ ). Other driving mechanisms such as magnetorotationally (Metzger et al. 2007; Winteler et al. 2012) or acoustic-wave driven outflows are beyond the scope of this Letter and cannot be excluded as the  $r$ -process ori-

gins on the basis of our result.

Neutrino-driven PNS winds are, however, promising sources that eject light trans-iron elements made in QSE (Sr, Y, and Zr) and by a weak  $r$ -process (up to Pd, Ag, and Cd), in addition to the early convective ejecta of CCSNe (Wanajo et al. 2011a). If not the main origin of the  $r$ -process elements beyond  $A \sim 110$ , they could be the sources of low-level abundances of Sr and Ba (e.g.,  $[(\text{Sr}, \text{Ba})/\text{Fe}] < -1$ ) found in extremely metal-poor stars. Future surveys or indications of massive NSs, long-term hydrodynamical simulations of PNS winds, and galactic chemical evolution studies will be important to make clear the role of PNS winds in the enrichment histories of galaxies.

This work was supported by the JSPS Grants-in-Aid for Scientific Research (23224004).

#### REFERENCES

- Aoki, W., Suda, T., Boyd, R. N., Kajino, T., & Famiano, M. A. 2013, *ApJ*, 766, L13
- Arcones, A., Janka, H.-Th., & Scheck, L. 2006, *A&A*, 467, 1227
- Arcones, A. & Montes, F. 2011, *ApJ*, 731, 5
- Boyd, R. N., Famiano, M. A., Meyer, B. S., Motizuki, Y., Kajino, T., & Roederer, I. U. 2012, *ApJ*, 744, L14
- Cardall, C. Y. & Fuller, G. M. 1997, *ApJ*, 486, L111
- Cybert, R. H., et al. 2010, *ApJS*, 189, 240
- Demorest, P. B., Pennucci, T., Ransom, S. M., Roberts, M. S. E., & Hessels, J. W. T. 2010, *Nature*, 467, 1081
- Duncan, R., Shapiro, S. L., & Wasserman, I. 1986, *ApJ*, 309, 141
- Fischer, T., Whitehouse, S. C., Mezzacappa, A., Thielemann, F.-K., Liebendörfer, M. 2010, *A&A*, 517, 80
- Fischer, T., Martínez-Pinedo, G., Hempel, M., & Liebendörfer, M. 2012, *Phys. Rev. D*, 85, 083003
- Goriely, S., Chamel, N., Pearson, J. M. 2010, *Phys. Rev. C*, 82, 035804
- Hoffman, R. D., Woosley, S. E., & Qian, Y.-Z. 1997, *ApJ*, 482, 951
- Honda, S., Aoki, W., Ishimaru, Y., Wanajo, S., & Ryan, S. G. 2006, *ApJ*, 643, 1180
- Horowitz, C. J., Shen, G., O'Connor, E., & Ott, C. D. 2012, *Phys. Rev. C*, 86, 065806
- Hüdepohl, L., Müller, B., Janka, H.-Th., Marek, A., Raffelt, G. G. 2010, *Phys. Rev. Lett.*, 104, 251101
- Ishimaru, Y. & Wanajo, S. 1999, *ApJ*, 511, L33
- Janka, H.-T., Hanke, F., Hüdepohl, L., Marek, A., Müller, B., & Obergaulinger, M. 2012, *PTEP*, 01A309
- Kuroda, T., Wanajo, S., & Nomoto, K. 2008, *ApJ*, 672, 1068
- Lattimer, J. M. 2011, *Ap&SS*, 336, 67
- Martínez-Pinedo, G., Fischer, T., Lohs, A., & Huther, L. 2012, *Phys. Rev. Lett.*, 109, 251104
- McLaughlin, G. C., Fuller, G. M., & Wilson, J. R. 1996, *ApJ*, 472, 440
- Metzger, B. D., Thompson, T. A., & Quataert, E. 2007, *ApJ*, 659, 561
- Meyer, B. S., Mathews, G. J., Howard, W. M., Woosley, S. E., & Hoffman, R. D. 1992, *ApJ*, 399, 656
- Meyer, B. S., McLaughlin, G. C., & Fuller G. M. 1998, *Phys. Rev. C*, 58, 3696
- Otsuki, K., Tagoshi, H., Kajino, T., & Wanajo, S. 2000, *ApJ*, 533, 424
- Qian, Y.-Z. & Woosley, S. E. 1996, *ApJ*, 471, 331
- Qian, Y.-Z., Vogel, P., & Wasserburg, G. J. 1998, *ApJ*, 494, 285
- Reddy, S., Prakash, M., & Lattimer, J. M. 1998, *Phys. Rev. D*, 58, 013009
- Roberts, L. F. 2012, *ApJ*, 755, 126
- Roberts, L. F., Reddy, S., & Shen, G. 2012, *Phys. Rev. C*, 86, 065803
- Roederer, I. U., et al. 2012, *ApJS*, 203, 27
- Roederer, I. U. 2013, *AJ*, 145, 26
- Siqueira Mello Jr., et al. 2013, *A&A*, 550, A122
- Steiner, A. W., Lattimer, J. M., & Brown, E. F. 2013, *ApJ*, 765, L5
- Snedden, C., Cowan, J. J., & Gallino, R. 2008, *ARA&A*, 46, 241
- Suzuki, T. K. & Nagataki, S. 2005, *ApJ*, 628, 914
- Tachibana, T., Yamada, M., & Yoshida, Y. 1990, *Progr. Theor. Phys.*, 84, 641
- Takahashi, K., Wittit, J., & Janka, H.-T. 1994, *A&A*, 286, 857
- Timmes, F. X. & Swesty, F. D. 2000, *ApJS*, 126, 501
- Thompson, T. A., Burrows, A., & Meyer, B. S. 2001, *ApJ*, 562, 887
- Thompson, T. A. 2003, *ApJ*, 585, L33
- van Kerkwijk, M. H., Breton, R. P., & Kulkarni, S. R. 2011, *ApJ*, 728, 95
- Wanajo, S., Kajino, T., Mathews, G. J., & Otsuki, K. 2001, *ApJ*, 554, 578
- Wanajo, S. 2006, *ApJ*, 650, L79
- Wanajo, S. 2007, *ApJ*, 666, L77
- Wanajo, S., Janka, H.-T., & Müller, B. 2011, *ApJ*, 726, L15
- Wanajo, S., Janka, H.-T., & Kubono, S. 2011, *ApJ*, 729, 46
- Winteler, C., et al. 2012, *ApJ*, 750, L22
- Woosley, S. E., Wilson, J. R., Mathews, G. J., Hoffman, R. D., & Meyer, B. S. 1994, *ApJ*, 433, 229
- Xu, Y., Goriely, S., Jorissen, A., Chen, G. L., & Arnould, M. 2013, *A&A*, 549, 106